Figure 4 Time–space domains of glacial landform formation. Distance is shown along a transect from dispersal centre to ice margin. Time is shown from the LGM to the time of deglaciation at the final dispersal centre. Bars at the top of the figure show along-transect location of landform types and relict landscapes.

sedimentary cover rocks, the main source of fine-grained sea-floor diamicts in the region. Whether or not these diamicts were deformable (and therefore conductive to low ice-sheet profiles) was a function of ice-sheet basal temperatures in this region, and cannot be assumed *a priori*. Horsts of Precambrian rock (Nottingham, Salisbury and Mill islands, and the northern part of Southampton island) stand 200–600 m above the adjacent sea floor and may have acted as frozen-bed 'sticky spots'[29] in a region elsewhere characterized by thawed-bed conditions, thereby substantially retarding ice outflow through the Hudson Strait and raising the surface elevations over Hudson Bay. This is a situation analogous to the Åland islands in the FIS area, which modelling experiments indicate to have been frozen-bed sticky spots hindering headward propagation of the Baltic ice stream into the central Fennoscandian ice sheet area[30].

Our results show that a time-dependent basal thermal evolution was the primary control on bed traction in each of the FIS and LIS areas. Large fractions of the LIS and FIS beds were frozen, but thawed during the post-LGM stages. This created the conspicuous landform ribbed moraine, and efficiently lowered ice-sheet profiles by allowing basal sliding and deformation of formerly frozen and undeformable till. □

1. Denton, G. H. & Hughes, T. J. (eds) *The Last Great Ice Sheets* (Wiley-Interscience, New York, 1981).
2. Budd, W. F. & Smith, I. N. in *Sea Level, Ice, and Climatic Change* (ed. Allison, I.) 369–409 (Publ. 131, International Association of Hydrological Sciences, Washington DC, 1981).
3. Licciardi, J. M., Clark, P. U., Jenson, J. W. & MacAyeal, D. R. Deglaciation of a soft-bedded Laurentide Ice Sheet. *Quat. Sci. Rev.* **17**, 427–448 (1998).
4. MacAyeal, D. R. Binge/purge oscillations of the Laurentide Ice Sheet as a cause of the North Atlantic's Heinrich events. *Paleoceanography* **8**, 775–784 (1993).
5. Hooke, R. LeB. Basal temperatures in polar ice sheets - a qualitative review. *Quat. Res.* **7**, 1–13 (1977).
6. Hughes, T. J. in *Proc. 2nd Int. Conf. on Permafrost* 213–223 (National Academy of Sciences, Washington DC, 1973).
7. Boulton, G. S. in *Drumlin Symposium* (eds Menzies, J. & Rose, J.) 25–80 (Balkema, Rotterdam, 1987).
8. Lundqvist, J. Rogen moraine - an example of two-step formation of glacial landscapes. *Sedim. Geol.* **111**, 27–40 (1997).
9. Boulton, G. S. & Clark, C. D. A highly mobile Laurentide Ice Sheet revealed by satellite images of glacial lineations. *Nature* **346**, 813–817 (1990).
10. Prest, V. K., Grant, D. R. & Rampton, V. N. *Glacial Map of Canada* (Geological Survey of Canada, Ottawa, 1969).
11. Lagerbäck, R. & Robertsson, A. -M. Kettle holes - Stratigraphical archives for Weichselian geology and palaeoenvironment in northernmost Sweden. *Boreas* **17**, 439–468 (1988).
12. Bouchard, M. A. Subglacial landforms and deposits in central and northern Quebec, Canada, with emphasis on Rogen moraines. *Sedim. Geol.* **62**, 293–308 (1989).
13. Aylsworth, J. M. & Shilts, W. W. Glacial features around the Keewatin ice divide: Districts of Mackenzie and Keewatin. *Geol. Surv. Can. Pap.* **88-24**, 1–21 (1989).
14. Hättestrand, C. Ribbed moraines in Sweden - distribution pattern and paleoglaciological implications. *Sedim. Geol.* **111**, 41–56 (1997).
15. Hättestrand, C. & Kleman, J. Ribbed moraine formation. *Quat. Sci. Rev.* **18**, 43–61 (1999).
16. Hutter, K. & Olunloyo, V. O. S. Basal stress concentrations due to abrupt changes in boundary conditions: a cause for high till concentration at the bottom of a glacier. *Ann. Glaciol.* **2**, 29–33 (1981).
17. Kleman, J. & Borgström, I. Glacial land forms indicative of a partly frozen bed. *J. Glaciol.* **40**, 255–264 (1994).
18. Kleman, J. Preservation of landforms under ice sheets and ice caps. *Geomorphology* **9**, 19–32 (1994).
19. Dyke, A. S. Landscapes of cold-centred Late Wisconsinan ice caps, Arctic Canada. *Prog. Phys. Geogr.* **17**, 223–247 (1993).
20. Sugden, D. E. & Watts, S. H. Tors, felsenmeer and glaciation in northern Cumberland Peninsula, Baffin Island. *Can. J. Earth Sci.* **14**, 2817–2823 (1977).
21. Kleman, J., Borgström, I. & Hättestrand, C. Evidence for a relict glacial landscape in Quebec-Labrador. *Palaeogeogr. Palaeoclimatol. Palaeoecol.* **111**, 217–228 (1994).
22. Dyke, A. S., Morris, T. F., Green, D. E. C. & England, J. *Quaternary Geology of Prince of Wales Island Arctic Canada* (Mem. 433, Geological Survey of Canada, Ottawa, 1992).
23. Nordkalott project *Map of Quaternary Geology* Sheet 2, *Glacial Geomorphology, Northern Fennoscandia, 1:1 mill.* (Geological Surveys of Finland, Norway and Sweden, Geological Survey of Sweden, Uppsala, 1986).
24. Sollid, J. L. & Torp, B. *Nasjonalatlas for Norge, Glacialgeologisk kart over Norge, 1:1 mill.* (Geografisk Institutt, Oslo, 1984).
25. Heine, J. T. & McTigue, D. F. A case for cold-based continental ice sheets—A transient thermal model. *J. Glaciol.* **42**, 37–42 (1996).
26. Huybrechts, P. & T'siobbel, S. Thermomechanical modeling of Northern Hemisphere ice sheets with a two-level mass-balance parametrization. *Ann. Glaciol.* **21**, 111–116 (1995).
27. Fisher, D. A. *et al.* Penny ice cap cores, Baffin Island, Canada, and the Wisconsin fore dome connection: Two states of Hudson Bay ice cover. *Science* **279**, 692–695 (1998).
28. Kleman, J., Hättestrand, C., Borgström, I. & Stroeven, A. Fennoscandian palaeoglaciology reconstructed using a glacial geological inversion model. *J. Glaciol.* **43**, 283–299 (1997).
29. Hughes, T. J. Can ice sheets trigger abrupt climatic change? *Arct. Alp. Res.* **28**, 448–465 (1996).
30. Holmlund, P. & Fastook, J. A time-dependent glaciological model of the Weichselian Ice Sheet. *Quat. Int.* **27**, 53–58 (1995).
31. Niemelä, J., Ekman I. & Lukashov, A. (eds) *Quaternary Deposits of Finland and Northwestern part of Russian Federation and their Resources 1:1 mill* (Geological Survey of Finland, and Institute of Geology, Karelian Science Centre of the Russian Academy of Sciences, Helsinki, 1993).

Limits on differential rotation of the inner core from an analysis of the Earth's free oscillations

Gabi Laske & Guy Masters

Institute of Geophysics and Planetary Physics, University of California San Diego, 9500 Gilman Dr, La Jolla, California 92093-0225, USA

Differential rotation of the Earth's inner core has been inferred by several seismic 'body-wave' studies[1–6] which indicate that the inner core is rotating at a rate between 0.2° and 3° per year faster than the Earth's crust and mantle. The wide range in inferred rotation rate is thought to be caused by the sensitivity of body-wave studies to local complexities in inner-core structure[3,7]. Free-oscillation 'splitting functions', on the other hand, are insensitive to local structure and therefore have the potential to estimate differential rotation more accurately. A previous free-oscillation study[8], however, was equivocal in its conclusions because of the relatively poor quality and coverage of the long-period digital data available 20 years ago. Here we use a method for analysing free oscillations[9] which is insensitive to

earthquake source, location and mechanism to constrain this differential rotation. We find that inner-core differential rotation is essentially zero over the past 20 years (to within ±0.2° per year), implying that the inner core is probably gravitationally locked to the Earth's mantle[10].

It has long been known that free oscillations which sample the inner core are strongly split[11] by a structure which is dominantly axisymmetric and mimics the effect of an excess ellipticity of the Earth. In 1986, workers at Harvard[12,13] inferred that anisotropy of the inner core was the main reason for the anomalous splitting and this same anisotropy could explain some features of the travel times of body waves which sample this region[14]. This explanation has become generally accepted by seismologists though agreement on the physical cause for the phenomenon has been lacking[15–18]. According to the accepted story, the inner core behaves roughly like a single anisotropic crystal with a seismically fast symmetry axis closely aligned with the rotation axis of the Earth. A small departure of the fast symmetry axis from the rotation axis has been inferred by several groups[19–22]; this departure implies that any differential rotation of the inner core would result in temporal variations of the travel times of body waves emanating from a particular source region and recorded by a particular receiver. Such temporal variations have been inferred to exist for some paths[1,3] but not for others[5]. Furthermore, detailed studies of body-wave arrival times using arrays of detectors have shown that strong local lateral variations in anisotropy in the inner core exist, making it much more difficult to infer a differential rotation rate for the inner core.

Free oscillation splitting functions provide a much better tool for looking at the differential rotation rate of the inner core. Free oscillations are natural low-pass filters of three-dimensional structure, so it is efficient to use a spherical harmonic expansion of structure in mode studies. By this, we mean that structure is expanded in the form

$$\delta\mathbf{m}(r,\theta,\phi) = \sum_{s,t} \delta\mathbf{m}_s^t(r)Y_s^t(\theta,\phi)$$

where $Y_s^t = X_s^t(\theta)e^{im\phi}$ is a spherical harmonic of harmonic degree s and azimuthal order number t; r, θ, ϕ are radius, co-latitude and longitude. Here, $\delta\mathbf{m}$ refers to lateral variations in density and seismic velocities. An isolated mode of harmonic degree s is sensitive to even-order structure only up to harmonic degree $2s$. Thus, modes of harmonic degree 1 are sensitive only to structure of degree 2. Unfortunately, it seems that structure of degree 2 in the inner core is almost completely zonal (azimuthal order = 0) as sensed by modes of harmonic degree 1, so such modes are insensitive to any rotation about the pole. Fortunately, other modes of harmonic degrees greater than 1 appear to be sensitive indicators of inner-core rotation.

We have recently introduced a new technique for analysing the sensitivity of a free oscillation to three-dimensional structure[9], which is independent of the source mechanism which excites the free oscillation. Briefly, for a particular earthquake and a mode of harmonic degree l, there are $2l+1$ linear combinations of recordings $\mathbf{b}(t)$ which we call 'receiver strips' which satisfy the following autoregressive relationship:

$$\mathbf{b}(t+\delta t) = P(\delta t)\mathbf{b}(t) \quad (1)$$

Here the matrix $P(\delta t) = \exp[i\delta t(H + I\bar{\omega})]$, $\bar{\omega}$ is the degenerate frequency of the mode, I is the identity matrix and H is the splitting matrix given by[23,24] (after corrections for the rotation and ellipticity of the Earth)

$$H_{mn} = \sum_{st} \gamma_{mn}^{st} c_s^t \quad (2)$$

where γ represents geometrical factors which can easily be computed, and

$$c_s^t = \int_0^a M_s(\mathbf{r}) \cdot \delta\mathbf{m}_s^t(r)r^2 \, dr$$

We note that each c_s^t is proportional to a depth-weighted average of a $\delta\mathbf{m}_s^t(r)$ where the weighting kernel, $M_s(r)$, varies from mode to mode. Hence, it is convenient to visualize the geographical distribution of structure sensed by a mode by forming the
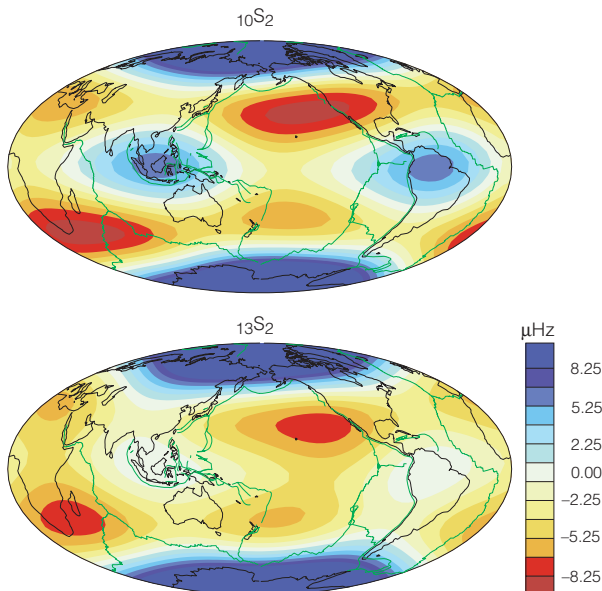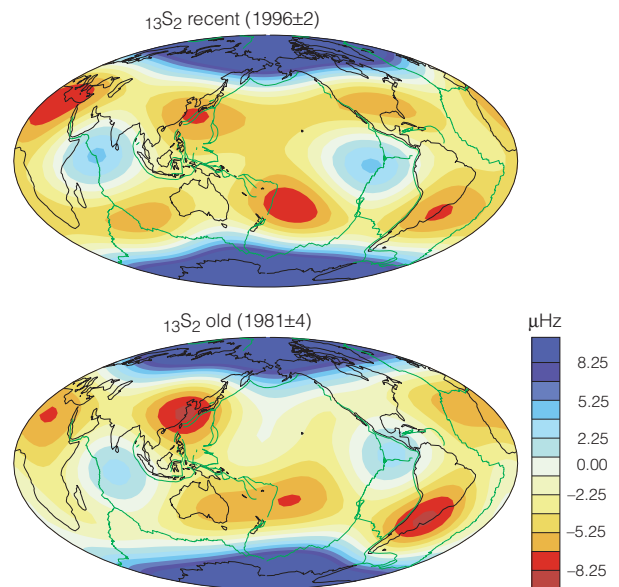

Figure 1 Splitting functions for the two modes $_{10}S_2$ and $_{13}S_2$. The effects of rotation and ellipticity have been removed before the inversion for structure coefficients (equation (2)). The splitting functions are very robust and the non-zonal patterns are very well aligned.

Figure 2 Splitting functions for mode $_{13}S_2$. Panel **a** uses recent events from the years 1996 ± 2, and panel **b** uses earlier events from the years 1981 ± 4. The effects of rotation and ellipticity have been removed before the inversion for structure coefficients, and the contribution of the mantle[31] has been removed. The anomalies shown are due to structure in the inner core. A westward rotation of the lower map about the vertical axis of 4.5° optimally aligns it with the upper map. Provided that our mantle correction is accurate, this comparison implies a westward inner-core rotation of 0.3° per year.
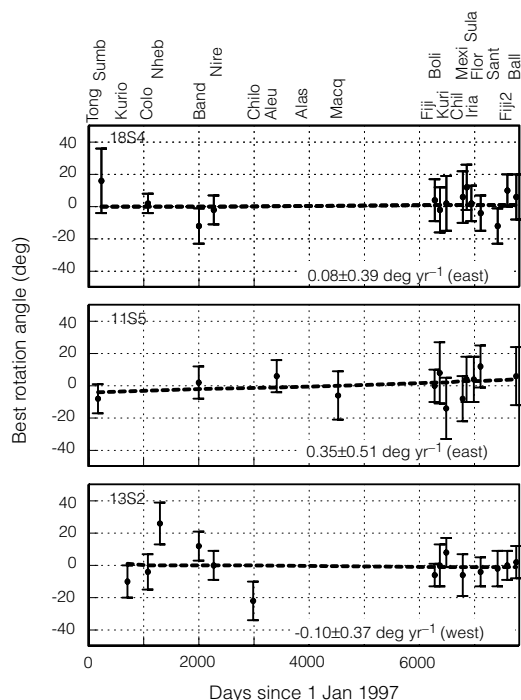
Figure 3 Time-dependent inner-core rotation angles. The angles, shown for the three modes $_{18}S_4$, $_{11}S_5$ and $_{13}S_2$, give the best fit to the receiver strips (see text) of individual events. The dashed lines fit the data in a least-squares sense. Their slopes translate to the annual rotation rates given in the lower right corner of each diagram. Positive rotation rates imply a superrotation of the inner core.

splitting function[25]:

$$f(\theta, \phi) = \sum_{s,t} c_s^t Y_s^t(\theta, \phi).$$

Our technique uses a linear inverse to estimate P from equation (1) by simultaneously fitting the receiver strips from many earthquakes. Matrix H can easily be recovered from P. We then solve another linear inverse problem to obtain the structure coefficients (equation (2)) and so form splitting functions. Splitting functions for two harmonic degree 2 modes which are sensitive to the inner core are shown in Fig. 1. These splitting functions have been derived using data from 11 large earthquakes which occurred between 1994 and 1998 (Table 1), and have been constructed using about 1,000 vertical component recordings. The measured splitting functions are exceptionally robust and exhibit non-zonal patterns which, interestingly, coincide geographically to better than a degree for the two modes. We take this as a measure of the precision of splitting functions that can be achieved using modern data.

For a mode sensitive to the inner core, a differential rotation will cause the non-zonal structure coefficients to change with time so the splitting function will change with time. We illustrate this idea with the mode $_{13}S_2$ (Fig. 2). We compare the splitting function derived using our technique and recent data (top panel) with the splitting function obtained employing the traditional, nonlinear technique of iterative spectral fitting[26,27] applied to data covering the timespan 1977−85[27,28]. We compare the splitting functions after correction for structure in the mantle which we do not expect to change with time. This mantle contribution has been estimated using several different models of mantle structure[29–31] and appears to be robustly determined. However, it contributes substantially to the patterns shown in Fig. 1 and, in fact, the mantle can explain all the non-zonal signals we see for modes of harmonic degree 1 (for example, $_8S_1$, $_{13}S_1$), making these modes useless for determining inner-core rotation.

If we solve for an inner-core rotation that best fits the two mantle-corrected non-zonal patterns for $_{13}S_2$, we find that the best answer
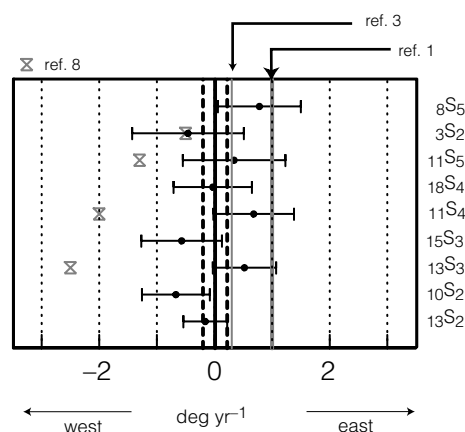

Figure 4 Inner-core rotation rates obtained for nine core-sensitive modes. Also shown is the mean rotation rate, 0.01 ± 0.21 deg yr^{-1}, obtained from averaging over all modes. Dashed lines mark the error bars of the average. The hour-glass symbols mark the results of a recent mode study[8], and two grey vertical lines stand for the superrotations found in recent body-wave studies[1,3]. Our data are marginally consistent with a superrotation of 0.3° per year, though a superrotation of 1° per year is clearly inconsistent for most of the modes. See Table 1 for event abbreviations.

for the total pattern is an annual inner-core rotation of about 0.3° westward, though the weak non-zonal degree 2 part appears to go eastward while the stronger degree 4 part goes westward. Of course, this is physically impossible if the inner core is moving as a rigid body. This result is most likely to be due to errors in the older splitting function which is constrained by much fewer high-quality data than the modern one.

A better way of testing for inner-core rotation is by testing the hypothesis that the inner core is differentially rotating about the rotation axis. We assume that the modern data accurately constrain the current splitting function of the mode, and that we can properly correct for structure in the mantle. The corrected splitting function by assumption reflects only inner-core structure, which can now be rotated about the rotation axis using an assumed rotation rate. We then add the mantle contribution back in, and we have a synthetic H from which we compute a synthetic P. This P is used in equation (1) to test if the assumed rotation rate provides a good fit to the receiver strips, **b**, for any event. The data have to meet certain criteria to be considered in the hypothesis test. For example, the fit to the receiver strips with any non-zero inner-core rotation must be better than that using no rotation, and the receiver strips should be fitted close to their error bars. Not all events excite all modes, so we restrict

Table 1 Earthquakes used in this study

Event name	Year.day	Depth (km)	Moment (10^{20} Nm)	No. of records	Abbreviation
Balleny Islands region	1998.084	33	18.2	81	Ball
Fiji	1997.287	166	4.6	88	Fiji2
Santa Cruz Islands	1997.111	33	4.4	96	Sant
Flores	1996.169	587	7.3	90	Flor
Irian Jaya	1996.048	33	24.1	103	Iria
Sulawesi	1996.001	24	7.8	91	Sula
Mexico	1995.282	33	11.5	96	Mexi
Chile	1995.211	46	12.2	111	Chil
Kuril Islands	1994.277	54	30.0	101	Kuri
Bolivia	1994.160	631	26.3	88	Boli
Fiji	1994.068	562	3.1	72	Fiji
Macquarie Island	1989.143	10	13.6	52	Macq
Alaska	1987.334	10	7.3	41	Alas
Aleutians	1986.127	33	10.4	42	Aleu
Chile	1985.062	33	10.3	29	Chilo
New Ireland	1983.077	70	4.6	32	Nire
Banda Sea	1982.173	450	1.8	21	Band
New Hebrides	1980.199	33	4.8	21	Nheb
Colombia	1979.346	24	16.9	26	Colo
Kuril Islands	1978.340	91	6.4	24	Kurio
Sumbawa	1977.231	33	35.9	18	Sumb
Tonga	1977.173	65	13.9	16	Tong.

attention to those events which give a variance reduction greater than 70%. Most core-sensitive modes are also sensitive to mantle structure. Some events yield significantly different rotation angles for different mantle corrections[29,30]. We regard this as an indication of serious noise contamination, and discard these events for a particular mode. This conservative choice sometimes results in very few events to constrain the rotation rate for individual modes; for example, only nine events constrain the rate for mode $_3S_2$, and the rotation rate determined for this mode is less certain. We plot the apparent rotation angles for several modes as a function of event date (Fig. 3). The error bars represent the range of angles over which the fit to the receiver strips is adequate. The best-fitting straight line is also indicated, along with the corresponding apparent rotation rate.

For the hypothesis to be acceptable, all the modal splitting functions should appear to be rotating at the same rate. Figure 4 summarizes our best estimate of each mode's rotation rate. Also shown are the results of another recent mode study[8] and body-wave studies[1,3]. Even though some of the modes shown in Fig. 4 indicate significantly non-zero rotation rates (some indicate a slight westward inner-core rotation), these rates do not agree with each other. The mean rotation rate for all modes in our study is $0.01 \pm 0.21°$ per year, which is obviously insignificantly different from zero. The results shown are obtained using model SB10L18[30] to perform the mantle corrections, but other models give rather similar results ($0.03 \pm 0.21°$ per year for S16B30[29]. Recent body-wave analyses suggest that the rotation rate may be as small as $0.2-0.3°$ per year in an eastward sense. Such a rotation rate (also indicated in Fig. 4) is marginally consistent with most modes. We can certainly rule out a rate of $1°$ eastward, as well as a significant westward rotation. Perhaps complexity near the ray turning points or systematic changes in earthquake location procedures could allow smaller rotation rates to be compatible with the body-wave data.

We believe that a model analysis is the best way to determine inner-core rotation. First, we are dealing with large-scale vibrations which are insensitive to errors in event locations and to local structure in the inner core. Second, the method is independent of the earthquake source mechanism. Third, we do not need to worry about how much of the splitting functions we observe are caused by heterogeneity or anisotropy—all we care about is whether they change with time. Our results are marginally consistent with the small rotation rates reported in most recent body-wave analyses, though our best value indicates that the inner core is not rotating at a significant rate relative to the mantle. This would be in accord with the notion that the inner core is gravitationally locked to the mantle[10]. □

1. Song, X. & Richards, P. G. Seismological evidence for differential rotation of the Earth's inner core. *Nature* **382,** 221–224 (1996).
2. Su, W., Dziewonski, A. M. & Jeanloz, R. Planet within a planet: rotation of the inner core of the Earth. **274,** 1883–1887 (1996).
3. Creager, K. C. Inner core rotation rate from small-scale heterogeneity and time-varying travel times. *Science* **278,** 1248–1288 (1997).
4. Souriau, A. Earth's inner core—is the rotation real? *Science* **281,** 55–56 (1998).
5. Souriau, A. New seismological constraints on differential rotation rates of the inner core from Novaya Zemlya events recorded at DRV, Antarctica. *Geophys. J. Int.* **134,** F1–F5 (1998).
6. Souriau, A., Roudil, P. & Moynot, B. Inner core differential rotation: facts and artefacts. *Geophys. Res. Lett.* **24,** 2103–2106 (1997).
7. Creager, K. C. Large-scale variations in inner core anisotropy. *J. Geophys. Res.* (in the press).
8. Sharrock, D. S. & Woodhouse, J. H. Investigation of time dependent inner core structure by the analysis of free oscillation spectra. *Earth Planets Space* **50,** 1013–1018 (1998).
9. Masters, G., Laske, G. & Gilbert, F. Autoregressive estimation of the splitting matrix of free-oscillation multiplets. *J. Geophys. Res.* (submitted).
10. Buffet, B. A. A mechanism for decade fluctuations in the length of day. *Geophys. Res. Lett.* **23,** 3803–3806 (1996).
11. Masters, G. & Gilbert, F. Structure of the inner core inferred from observations of its spheroidal shear modes. *Geophys. Res. Lett.* **8,** 569–571 (1981).
12. Woodhouse, J. H., Giardini, D. & Li, X.-D. Evidence for inner core anisotropy from free oscillations. *Geophys. Res. Lett.* **13,** 1549–1552 (1986).
13. Morelli, A., Dziewonski, A. M. & Woodhouse, J. H. Anisotropy of the inner core inferred from *PKIKP* travel times. *Geophys. Res. Lett.* **13,** 1545–1548 (1986).
14. Poupinet, G., Pillet, R. & Souriau, A. Possible heterogeneity of the earth's core deduced from *PKIKP* travel times. *Nature* **305,** 204–206 (1983).
15. Jeanloz, R. & Wenk, H.-R. Convection and anisotropy of the inner core. *Geophys. Res. Lett.* **15,** 72–75 (1988).
16. Karato, S. Inner core anisotropy due to magnetic field-induced preferred orientation of iron. *Science* **262,** 1708–1711 (1993).
17. Yoshida, S., Sumita, I. & Kumazagawa, M. Growth model of the inner core coupled with the outer core dynamics and the resulting elastic anisotropy. *J. Geophys. Res.* **101,** 28085–28103 (1997).
18. Bergman, M. I. Measurements of elastic anisotropy due to solidification texturing and the implications for the Earth's inner core. *Nature* **389,** 60–63 (1997).
19. Su, W-J. & Dziewonski, A. M. Inner core anisotropy in three dimensions. *J. Geophys. Res.* **100,** 9831–9852 (1995).
20. Shearer, P. M. & Toy, K. M. *PKP(BC)* versus *PKP(DF)* differential travel times and aspherical structure in Earth's inner core. *J. Geophys. Res.* **96,** 2233–2247 (1991).
21. McSweeney, T. J., Creager, K. C. & Merrill, R. T. Depth extent of inner core seismic anisotropy and implications for geomagnetism. *Phys. Earth. Planet. Inter.* **101,** 131–156 (1997).
22. Song, X. Anisotropy of the Earth's inner core. *Rev. Geophys.* **35,** 297–313 (1997).
23. Woodhouse, J. H. The coupling and attenuation of nearly resonant multiplets in the earth's free oscillation spectrum. *Geophys. J. R. Astron. Soc.* **61,** 261–283 (1980).
24. Woodhouse, J. H. & Dahlen, F. A. The effect of a general aspherical perturbation on the free oscillations of the earth. *Geophys. J. R. Astron. Soc.* **53,** 335–354 (1978).
25. Woodhouse, J. H. & Giardini, D. Inversion for the splitting function of isolated low order normal mode multiplets. *Eos* **66,** 300 (1985).
26. Ritzwoller, M., Masters, G. & Gilbert, F. Observations of anomalous splitting and their interpretation in terms of aspherical structure. *J. Geophys. Res.* **91,** 10203–10228 (1986).
27. Giardini, D., Li, X.-D. & Woodhouse, J. H. Splitting functions of long period normal modes of the earth. *J. Geophys. Res.* **93,** 13716–13742 (1988).
28. Li, X.-D., Giardini, D. & Woodhouse, J. H. Large-scale three-dimensional even-degree structure of the Earth from splitting of long-period normal modes. *J. Geophys. Res.* **96,** 551–577 (1991).
29. Masters, G., Johnson, S., Laske, G. & Bolton, H. A shear velocity model of the mantle. *Phil. Trans. R. Soc. Lond. A* **354** 1385–1411 (1996).
30. Masters, G., Bolton, H. & Laske, G. Joint seismic tomography for P and S velocities: how pervasive are chemical anomalies in the mantle? *Eos* **80,** S14 (1999).

••

Environmental warming alters food-web structure and ecosystem function

Owen L. Petchey, P. Timon McPhearson, Timothy M. Casey & Peter J. Morin

Department of Ecology, Evolution and Natural Resources, 14 College Farm Road, Cook College, Rutgers University, New Brunswick, New Jersey 08901-8511, USA

••

We know little about how ecosystems of different complexity will respond to global warming[1–5]. Microcosms permit experimental control over species composition and rates of environmental change. Here we show using microcosm experiments that extinction risk in warming environments depends on trophic position but remains unaffected by biodiversity. Warmed communities disproportionately lose top predators and herbivores, and become increasingly dominated by autotrophs and bacterivores. Changes in the relative distribution of organisms among trophically defined functional groups lead to differences in ecosystem function beyond those expected from temperature-dependent physiological rates. Diverse communities retain more species than depauperate ones, as predicted by the insurance hypothesis, which suggests that high biodiversity buffers against the effects of environmental variation because tolerant species are more likely to be found[6,7]. Studies of single trophic levels clearly show that warming can affect the distribution and abundance of species[2,4,5], but complex responses generated in entire food webs greatly complicate inferences based on single functional groups.

We used microcosms containing aquatic microbes to investigate